

Small-scale magnetic and velocity inhomogeneities in a sunspot light bridge

Rohan E. Louis*

Leibniz-Institut für Astrophysik Potsdam (AIP), An der Sternwarte 16, 14482 Potsdam, Germany

Abstract

High resolution spectro-polarimetric observations of a sunspot light bridge by *Hinode*, reveal small-scale inhomogeneities in the magnetic field and velocity. These inhomogeneities arise as a consequence of a weak, secondary lobe in the Stokes V profile which have a polarity opposite that of the sunspot and very large ($>5 \text{ km s}^{-1}$) Doppler velocities of both signs, suggesting two distinct types of magnetic anomalies. These two sets of inhomogeneities are highly time-dependent and appear exclusively in the upper half of the light bridge and only after the light bridge is completely formed. Both sets of inhomogeneities appear as patches and can be present independent of the other, next to one another, or spatially separated in a single scan. A two-component inversion of the corresponding spectral profiles indicate that the inhomogeneities occupy a very small fraction, amounting to less than 10%, of the resolution element. These structures are likely driven by small-scale magneto-convection where they could further interact with the overlying sunspot magnetic field to produce reconnection jets in the chromosphere.

Keywords: Sunspots, light bridges, magnetic fields, high resolution, photosphere, spectro-polarimetry

Received 8 June 2015 / Accepted 2 September 2015

1. Introduction

Light bridges (LBs) are conspicuous, bright structures in the umbrae of sunspots and pores and are typically present during the formation or fragmentation of spots (García de La Rosa, 1987). LBs can be regarded as either field-free intrusions of hot plasma in the gappy umbral magnetic field (Parker, 1979; Choudhuri, 1986), or manifestations of large-scale magneto-convection (Rimmele, 2008) in umbrae. The latter scenario is now widely, although not universally, accepted as being responsible for the fine structure and energy transport

*rlouis@aip.de

in sunspots. This in particular has been made possible from the advancement in numerical simulations (Schüssler & Vögler, 2006; Cheung et al., 2010), as well as high resolution observations from both the ground and space (Ortiz et al., 2010; Rouppe van der Voort et al., 2010; Ruiz Cobo & Asensio Ramos, 2013; Scharmer et al., 2013; Esteban Pozuelo et al., 2015). The interaction between umbral dots and intruding penumbral filaments, typically seen during light bridge formation (Katsukawa et al., 2007; Louis et al., 2012), lends further credence to magneto-convection in sunspots. In this sense, LBs represent a natural location where convective disruptions are more vigorous and apparent than in other parts of a sunspot. Such a disruption could produce magnetic inhomogeneities that might explain the pronounced chromospheric activity in LBs as reported in Louis et al. (2008) and recently in Louis et al. (2014a). In this paper I analyse small-scale magnetic anomalies in a sunspot LB using high resolution observations from *Hinode* (Kosugi et al., 2007).

2. Observations

High resolution observations of NOAA AR 11271 were acquired by the *Hinode* spectropolarimeter (SP; Ichimoto et al., 2008; Lites et al., 2013) on 2011 August 18–19. During these two days the SP took 14 scans (nine scans on August 18 and five scans on August 19) of the active region in the fast mode, each scan covering a field of view (FOV) of nearly $75'' \times 82''$. On August 18, the scans were taken at 11:00–11:16 UT, 11:20–11:36 UT, 11:40–11:56 UT, 18:12–18:28 UT, 18:32–18:48 UT, 18:52–19:08 UT, 19:12–19:28 UT, 19:32–19:48 UT, and 19:52–20:08 UT. The five SP scans on August 19 have a similar scan time of 16 min starting at 08:05 UT and ending at 10:21 UT. In the fast mode, the SP recorded the four Stokes profiles of the Fe I lines at 630 nm with a spectral sampling of 2.15 pm, a step width of $0''.29$, and a spatial sampling of $0''.32$ along the slit. The Level 0 data were reduced using standard routines included in the Solar-Soft package (Lites & Ichimoto, 2013). The active region traversed heliocentric angles of 42° to 30° between August 18 and 19.

3. Results

3.1. Anomalous Stokes profiles in the light bridge

Figure 1 shows a small LB in the south-eastern half of the leading sunspot in AR 11271 that forms during the early part of August 18. There is also an indication of a pronounced intrusion of penumbral filaments at the northern part of the umbra-penumbra boundary (white rectangle in Fig 1). The tip of these filaments extend into the umbra as diffuse umbral dots (left panel of Fig 1). Nearly 6.5 hr later a second LB forms, dividing the umbra into two nearly equal halves with one its ends coinciding with the intruding penumbral filaments described above, while its other end connects to the smaller southern LB. The larger LB in the sunspot is the object of interest for this paper. There are frequent transitions between formation and fragmentation over a period of

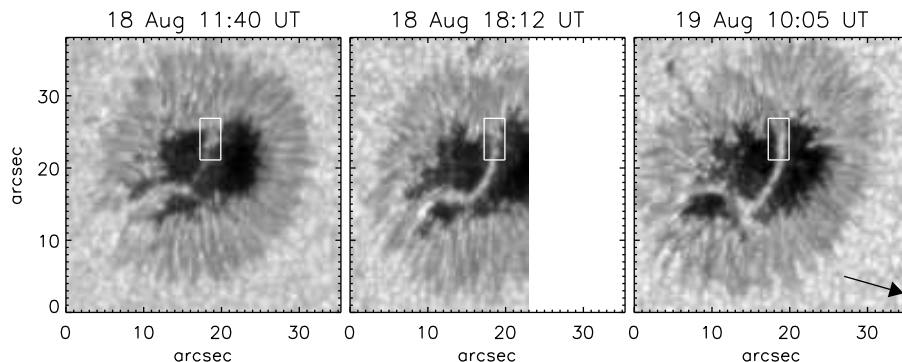


Figure 1: Continuum images of the leading sunspot in AR 11271 on 2011 August 18 and 19. The white rectangle depicts a 10×19 pixel FOV shown in Fig 2. The arrow in the right panel points to disk centre.

3 days, but the LB remains intact between the latter half of August 18 to the end of August 19 (Fig. 8 of [Louis et al. \(2014b\)](#)).

A smaller FOV consisting of the upper part of the LB is shown in Fig. 2, wherein the Stokes V profile at every pixel has been overlaid on the continuum map. Prior to the formation of the LB, the profiles consist of normal, anti-symmetric lobes (top left panel of Fig 2). However, after the LB is formed, there is a clear indication of two different kinds of anomalous profiles present in it. These are indicated in blue and red colours in Fig. 2 and will henceforth be referred to as blue profiles (BPs) and red profiles (RPs). These anomalous profiles comprise a weak, but discernible, second component and their name serves to distinguish their position with respect to the primary lobes of the V profile. It is to be noted that, although both sets of profiles have opposite Doppler (velocity) signatures, their signs are opposite to the primary lobes of the V profile. This would suggest offhand that the BPs and RPs have a polarity opposite that of the sunspot (see Sect. 3.2).

The amplitude of the secondary lobe in Stokes V , corresponding to the weak component in the BPs and RPs, is less than 5% (e.g. bottom panels of columns 1 and 2 in Fig.3). While the profiles indicated in the figure were selected by hand, it was verified that the amplitude of the weak lobe was at least four times the noise level of 1.5×10^{-3} . The peak corresponding to the BPs and RPs is, on an average, located at 17 pm and 22.5 pm, respectively from line centre. This suggests that the features are associated with very large doppler velocities. It is observed that the BPs and RPs are confined exclusively to the upper half of the LB throughout the observing period. These profiles appear in patches, sometimes as small as 0.2 arcsec^2 in area. The BPs and RPs can either appear i) completely independent of each other (panels 2 and 3), or ii) adjacent to each other (panels 4 and 5), or iii) separated from each other (panel 6). Since there are only limited SP scans it is difficult to establish the lifetimes of these features. As they can be sometimes seen in successive scans at/near the same

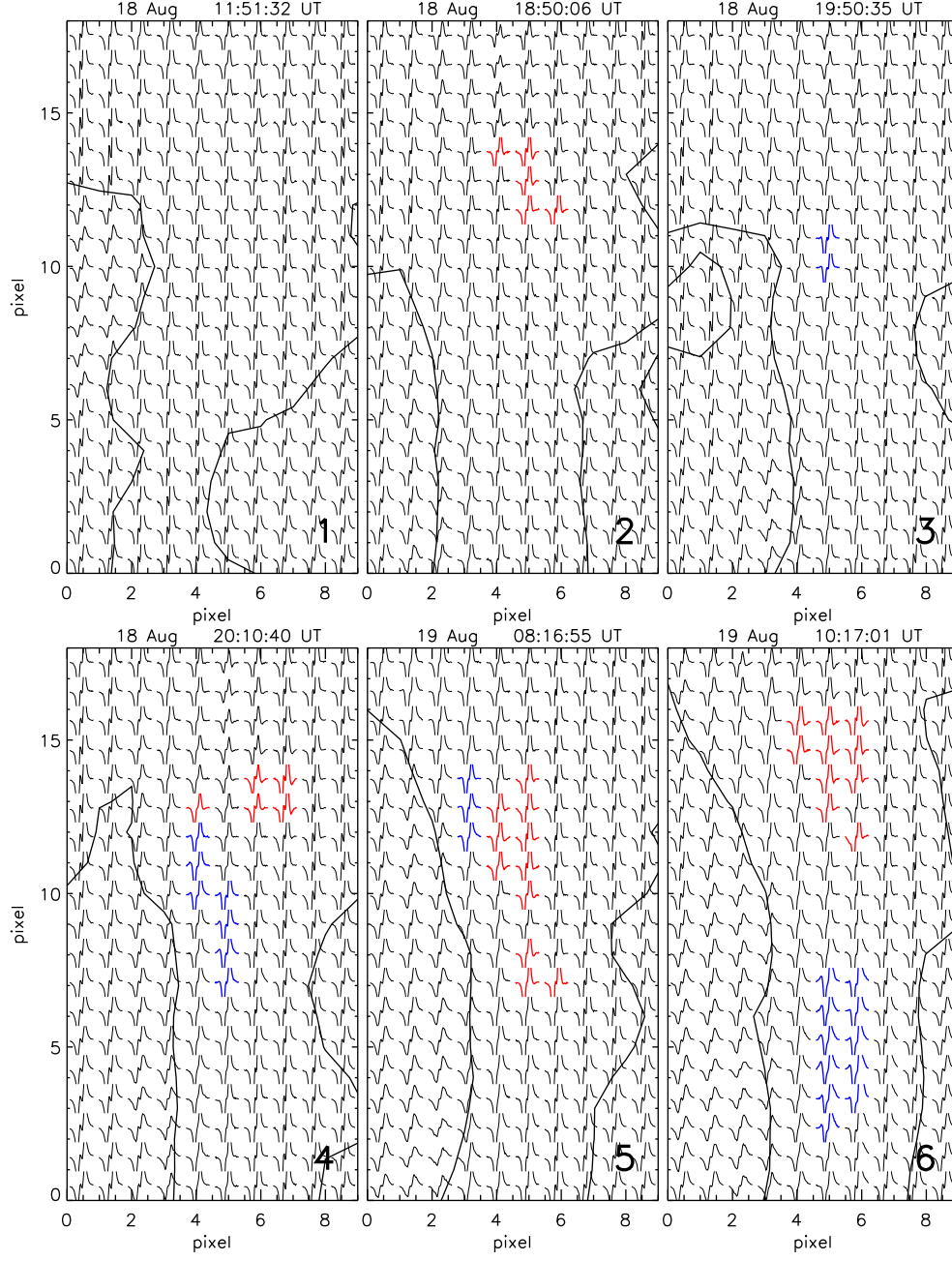


Figure 2: Stokes V profiles in the LB. The FOV corresponds to the white rectangle shown in Fig. 1. The black contour outlines the LB. The V profile corresponding to the Fe line at 630.25 nm is overlaid on each pixel and is scaled between $\pm 10\%$ of the QS continuum intensity. The blue (red) colours indicate that the weaker, second lobe is present on the blue-ward (red-ward) side of the primary lobe. The time indicated on the top of the panel represents the instant when the slit was at the left edge of the FOV.

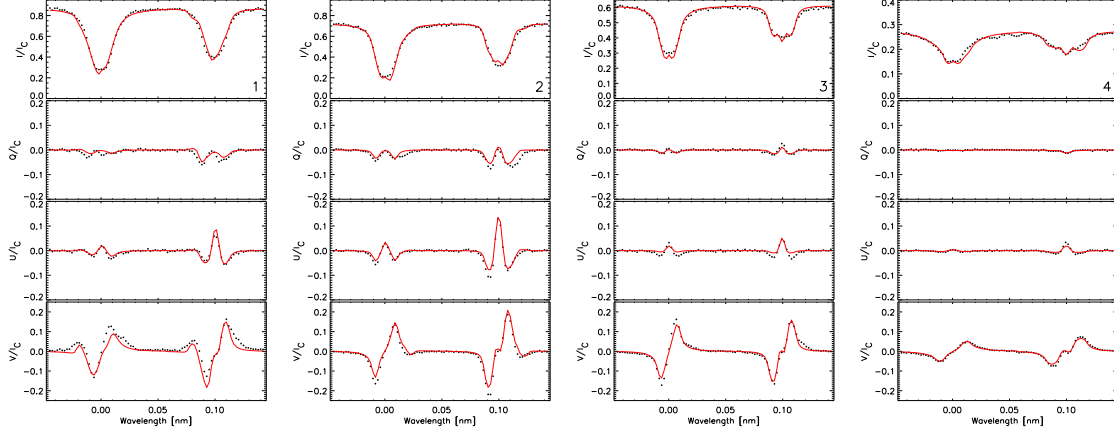


Figure 3: Results from SIR inversions. The *filled black circles* and *solid red line* represent the observed and synthetic spectra, respectively. From left to right: Stokes profiles corresponding to BP, RP, neighbouring pixel in LB, and an umbral pixel.

pixel, a lower limit of 20 min can be attributed to these features.

3.2. Magnetic field and LOS velocity associated with BPs and RPs

The BPs and RPs signify multiple components in the resolution element or gradients in the magnetic field and LOS velocity (Auer & Heasley, 1978). The physical parameters associated with these profiles were retrieved using Stokes Inversion based on Response functions (SIR; Ruiz Cobo & del Toro Iniesta, 1992). A typical BP and RP were inverted using a two-component model with height independent parameters except for temperature, which was perturbed with two nodes. Results of this inversion are shown in columns 1 and 2 of Fig. 3 which correspond to the BP and RP, respectively. Columns 3 and 4 represent fits to a neighbouring pixel in the light bridge and an umbral pixel, respectively, which were obtained using a single component inversion with height-independent parameters. Attempts were made with a single component inversion with gradients in the physical parameters but the resulting fits were unsatisfactory. Additionally, the two-component inversion was redone with height-dependent parameters, as described in Ruiz Cobo & Asensio Ramos (2013), but there was only a marginal improvement in the fit. The height-independent case allows a more simplistic interpretation of the physical scenario while still reproducing the spectral signatures specific to the anomalous profiles.

Table 1 shows that the second component, corresponding to the BP and RP, is characterised by Doppler velocities that are sub-sonic, but in excess of 5 km s^{-1} , and a polarity opposite that of the sunspot. A majority of the pixels in the LB which show normal Stokes V profiles also have the same polarity as the sunspot. In addition, one finds that the fill fraction of the second component to be around 10%, which represents the upper limit for these structures and the reason for the weak lobe in the profile. The field strength of the second

Table 1: Values of physical parameters obtained from SIR inversions. Field inclination is expressed in the local reference frame.

	BP	RP	LB	Umb
Field Strength [G]	1554	1581	1688	2611
	1535	1747	0	0
Field Inclination [deg]	150	145	156	164
	59	54	0	0
LOS Velocity [km s ⁻¹]	0.6	0.3	0.2	0.3
	-5.2	6.7	0.0	0.0
Fill Fraction	0.91	0.96	1.00	1.00
	0.09	0.04	0.00	0.00

component exceeds 1.5 kG and is comparable with the primary/main component which is also similar to other pixels in the LB.

3.3. Discussion

The anomalous profiles in the LB represent small-scale inhomogeneities in the magnetic field and velocity. These inhomogeneities have a polarity opposite that of the sunspot, including the LB, and have large Doppler-shifts of either sign. Their presence is detected by the weak, second component in the circular polarization profiles, which is clearly discernible, despite i) the reduced spatial resolution of the SP fast mode scan, and ii) not having corrected for spatially-induced polarized stray light arising from the point spread function of the *Hinode* telescope (van Noort, 2012). The reason these inhomogeneities stand out is because of their large Doppler shifts, the absence of which would have rendered them difficult to detect because of their small fill fraction, as they constitute less than 10% of the resolution element.

The anomalous Stokes profiles in a sunspot LB, reported by Louis et al. (2009), had the same polarity as the sunspot and were primarily associated with supersonic downflows, while those reported here have a polarity opposite that of the sunspot and have large Doppler shifts of either sign, that appear very close to one another and evolve on short time-scales. The red profiles in particular, are similar to those associated with the supersonic Evershed mass flux (Evershed, 1909) returning to the solar photosphere in the outer penumbra and beyond the sunspot boundary (Westendorp Plaza et al., 2001b,a; del Toro Iniesta et al., 2001; Bellot Rubio et al., 2004; Ichimoto et al., 2007; Beck, 2008).

An inspection of broad-band *Hinode* Ca II H filtergrams on August 18 reveal that small-scale chromospheric jets, seen the following day (Louis et al., 2014a), are only present after the LB is formed, i.e. after 18:00 UT, but not earlier in the day when the LB was only confined to an extended penumbral structure. Since the supersonic downflows detected by Louis et al. (2009) were also associated with strong chromospheric enhancements/jets, it strongly suggests a causal relationship between the small-scale inhomogeneities in a LB, irrespective of their

magnetic polarity and nature of the Doppler shift, and the dynamics in the overlying chromosphere.

The natural question that arises is, what produces these small-scale inhomogeneities. Considering that these features have large Doppler-shifts, a strong gas pressure gradient is needed to drive the plasma to these velocities. Furthermore, the pressure gradient ought to have opposite signs in order to produce both blue and redshifts. It is known that in the inner penumbra, penumbral grains exhibit an inward motion towards the umbra-penumbra boundary, which is observed both in intensity images as well as LOS velocity maps (Sobotka & Jurčák, 2009). This inward migration could explain the non-uniform, but predominantly unidirectional, flow directed from the northern end of the LB into its axis, as found by Louis et al. (2014a). Such flows would indicate the existence of a pressure gradient that could drive a flow along the axis of the LB, at least at the northern end or upper half of the LB, where the small-scale velocity and magnetic inhomogeneities are predominantly located. However, it is also known that penumbral grains are associated with blueshifts of around 1 km s^{-1} in the limb side penumbra (Rimmele & Marino, 2006). Thus, their motion and weakly subsonic speeds, leaves the presence of the strong redshifts in the LB, unexplained.

Recently Lagg et al. (2014) reported supersonic downflows at the edges of light bridge granules and suggested that these downflows reflect intense convection that arises from a combination of gravitational acceleration and radiative cooling at the interface of the umbra and the LB. However, the LB in question here has not evolved sufficiently to a granular stage and is still confined to the umbral environment, which is why the small-scale chromospheric jets are prevalent here and absent in the LB studied by Lagg et al. (2014). Furthermore, the redshifts reported here occur at different locations of the LB and often in its interior which would suggest that the magnetic and velocity inhomogeneities described here are likely produced by small-scale magneto-convection which would effectively produce both blue and redshifts. This is supported by the fact that the G-band images indicate the presence of a dark lane running along the axis of the LB (Figs. 1 and 2 of Louis et al. (2014a)), even though the resolution is insufficient to detect smaller granule/grain-like structures on the LB. However, the photospheric morphology of the LB investigated here is similar to the non-granular LB studied by Rouppe van der Voort et al. (2010), with the exception that they only detect upflows of around 1 km s^{-1} , along the dark lane, that are surrounded by relatively weaker downflows. Small-scale magneto-convection would also explain the opposite polarity magnetic elements in the LB which could reconnect with the overlying the sunspot magnetic field to produce the chromospheric jets. This scenario is also consistent with spectroscopic observations of Schleicher et al. (2003), where they found rapid variations of blue and redshifts extending over a large section of a LB. These variations, measuring nearly 1.5 km s^{-1} , occurred over a time scale of 35 s.

If small-scale magneto-convection is indeed responsible for these inhomogeneities it is necessary to determine how the physical parameters are stratified in geometrical height (Puschmann et al., 2010) and how the iso- τ layers are

arranged across the LB. Unfortunately, the significant height difference in the formation heights of the LB and the neighbouring umbra makes the estimation of such a geometrical height scale, solely from the photospheric Fe line pair, impossible and would necessitate the use of multiple spectral lines that form over a wide range of heights in the solar atmosphere. This would be possible with, for instance, the GREGOR Fabry-Pérot Interferometer (GFPI; [Puschmann et al., 2012](#)), where high resolution imaging spectro-polarimetric observations in two spectral lines can be performed quasi-simultaneously with sufficiently high spectral resolution.

3.4. Conclusions

The magnetic and velocity inhomogeneities in a sunspot light bridge are likely produced by magneto-convection that renders high-speed plasma flows at very small-spatial scales that also vary in time. The presence of these inhomogeneities could facilitate magnetic reconnection in the chromosphere with the overlying sunspot magnetic field and illustrates the complex magnetic topology associated with light bridges. Multi-wavelength, spectro-polarimetric observations with good spectral and high spatial resolution are necessary to confirm the magneto-convective origin of these small-scale inhomogeneities.

Acknowledgements. Hinode is a Japanese mission developed and launched by ISAS/JAXA, collaborating with NAOJ as a domestic partner and NASA and STFC (UK) as international partners. Scientific operation of the Hinode mission is conducted by the Hinode science team organized at ISAS/JAXA. This team mainly consists of scientists from institutes in the partner countries. Support for the postlaunch operation is provided by JAXA and NAOJ (Japan), STFC (UK), NASA, ESA, and NSC (Norway). I thank Horst Balthasar for reading the manuscript and providing useful comments and suggestions. I am grateful for the financial assistance from the German Science Foundation (DFG) under grant DE 787/3-1 and from SOLARNET—the European Commission’s FP7 Capacities Programme under Grant Agreement number 312495. I thank the referees for their useful comments and suggestions.

References

- Auer, L. H., & Heasley, J. N. (1978). The origin of broad-band circular polarization in sunspots. *A&A*, *64*, 67–71.
- Beck, C. (2008). A 3D sunspot model derived from an inversion of spectropolarimetric observations and its implications for the penumbral heating. *A&A*, *480*, 825–838. doi:[10.1051/0004-6361:20078409](#). [arXiv:0712.3168](#).
- Bellot Rubio, L. R., Balthasar, H., & Collados, M. (2004). Two magnetic components in sunspot penumbrae. *A&A*, *427*, 319–334. doi:[10.1051/0004-6361:20041277](#).
- Cheung, M. C. M., Rempel, M., Title, A. M., & Schüssler, M. (2010). Simulation of the Formation of a Solar Active Region. *ApJ*, *720*, 233–244. doi:[10.1088/0004-637X/720/1/233](#). [arXiv:1006.4117](#).
- Choudhuri, A. R. (1986). The dynamics of magnetically trapped fluids. I - Implications for umbral dots and penumbral grains. *ApJ*, *302*, 809–825. doi:[10.1086/164042](#).

- del Toro Iniesta, J. C., Bellot Rubio, L. R., & Collados, M. (2001). Cold, Supersonic Evershed Downflows in a Sunspot. *ApJ*, *549*, L139–L142. doi:[10.1086/319137](https://doi.org/10.1086/319137).
- Esteban Pozuelo, S., Bellot Rubio, L. R., & de la Cruz Rodríguez, J. (2015). Lateral Downflows in Sunspot Penumbra Filaments and their Temporal Evolution. *ApJ*, *803*, 93. doi:[10.1088/0004-637X/803/2/93](https://doi.org/10.1088/0004-637X/803/2/93). [arXiv:1502.02981](https://arxiv.org/abs/1502.02981).
- Evershed, J. (1909). Radial movement in sun-spots. *MNRAS*, *69*, 454.
- Garcia de La Rosa, J. I. (1987). Umbral dots - A case of penetrative convection between sunspot fragments. *Sol. Phys.*, *112*, 49–58. doi:[10.1007/BF00148486](https://doi.org/10.1007/BF00148486).
- Ichimoto, K., Lites, B., Elmore, D., Suematsu, Y., Tsuneta, S., Katsukawa, Y., Shimizu, T., Shine, R., Tarbell, T., Title, A., Kiyohara, J., Shinoda, K., Card, G., Lecinski, A., Streander, K., Nakagiri, M., Miyashita, M., Noguchi, M., Hoffmann, C., & Cruz, T. (2008). Polarization Calibration of the Solar Optical Telescope onboard Hinode. *Sol. Phys.*, *249*, 233–261. doi:[10.1007/s11207-008-9169-9](https://doi.org/10.1007/s11207-008-9169-9).
- Ichimoto, K., Shine, R. A., Lites, B., Kubo, M., Shimizu, T., Suematsu, Y., Tsuneta, S., Katsukawa, Y., Tarbell, T. D., Title, A. M., Nagata, S., Yokoyama, T., & Shimojo, M. (2007). Fine-Scale Structures of the Evershed Effect Observed by the Solar Optical Telescope aboard Hinode. *PASJ*, *59*, 593. doi:[10.1093/pasj/59.sp3.S593](https://doi.org/10.1093/pasj/59.sp3.S593).
- Katsukawa, Y., Yokoyama, T., Berger, T. E., Ichimoto, K., Kubo, M., Lites, B., Nagata, S., Shimizu, T., Shine, R. A., Suematsu, Y., Tarbell, T. D., Title, A. M., & Tsuneta, S. (2007). Formation Process of a Light Bridge Revealed with the Hinode Solar Optical Telescope. *PASJ*, *59*, 577. doi:[10.1093/pasj/59.sp3.S577](https://doi.org/10.1093/pasj/59.sp3.S577). [arXiv:0709.2527](https://arxiv.org/abs/0709.2527).
- Kosugi, T., Matsuzaki, K., Sakao, T., Shimizu, T., Sone, Y., Tachikawa, S., Hashimoto, T., Minesugi, K., Ohnishi, A., Yamada, T., Tsuneta, S., Hara, H., Ichimoto, K., Suematsu, Y., Shimojo, M., Watanabe, T., Shimada, S., Davis, J. M., Hill, L. D., Owens, J. K., Title, A. M., Culhane, J. L., Harra, L. K., Doschek, G. A., & Golub, L. (2007). The Hinode (Solar-B) Mission: An Overview. *Sol. Phys.*, *243*, 3–17. doi:[10.1007/s11207-007-9014-6](https://doi.org/10.1007/s11207-007-9014-6).
- Lagg, A., Solanki, S. K., van Noort, M., & Danilovic, S. (2014). Vigorous convection in a sunspot granular light bridge. *A&A*, *568*, A60. doi:[10.1051/0004-6361/201424071](https://doi.org/10.1051/0004-6361/201424071). [arXiv:1407.1202](https://arxiv.org/abs/1407.1202).
- Lites, B. W., Akin, D. L., Card, G., Cruz, T., Duncan, D. W., Edwards, C. G., Elmore, D. F., Hoffmann, C., Katsukawa, Y., Katz, N., Kubo, M., Ichimoto, K., Shimizu, T., Shine, R. A., Streander, K. V., Suematsu, A., Tarbell, T. D., Title, A. M., & Tsuneta, S. (2013). The Hinode Spectro-Polarimeter. *Sol. Phys.*, *283*, 579–599. doi:[10.1007/s11207-012-0206-3](https://doi.org/10.1007/s11207-012-0206-3).

- Lites, B. W., & Ichimoto, K. (2013). The SP_PREP Data Preparation Package for the Hinode Spectro-Polarimeter. *Sol. Phys.*, *283*, 601–629. doi:[10.1007/s11207-012-0205-4](https://doi.org/10.1007/s11207-012-0205-4).
- Louis, R. E., Bayanna, A. R., Mathew, S. K., & Venkatakrishnan, P. (2008). Dynamics of Sunspot Light Bridges as Revealed by High-Resolution Images from Hinode. *Sol. Phys.*, *252*, 43–54. doi:[10.1007/s11207-008-9247-z](https://doi.org/10.1007/s11207-008-9247-z).
- Louis, R. E., Beck, C., & Ichimoto, K. (2014a). Small-scale chromospheric jets above a sunspot light bridge. *A&A*, *567*, A96. doi:[10.1051/0004-6361/201423756](https://doi.org/10.1051/0004-6361/201423756). [arXiv:1406.0103](https://arxiv.org/abs/1406.0103).
- Louis, R. E., Beck, C., Mathew, S. K., & Venkatakrishnan, P. (2014b). Anomalous flows in a sunspot penumbra. *A&A*, *570*, A92. doi:[10.1051/0004-6361/201424112](https://doi.org/10.1051/0004-6361/201424112). [arXiv:1408.6690](https://arxiv.org/abs/1408.6690).
- Louis, R. E., Bellot Rubio, L. R., Mathew, S. K., & Venkatakrishnan, P. (2009). Supersonic Downflows in a Sunspot Light Bridge. *ApJ*, *704*, L29–L33. doi:[10.1088/0004-637X/704/1/L29](https://doi.org/10.1088/0004-637X/704/1/L29). [arXiv:0908.3465](https://arxiv.org/abs/0908.3465).
- Louis, R. E., Ravindra, B., Mathew, S. K., Bellot Rubio, L. R., Raja Bayanna, A., & Venkatakrishnan, P. (2012). Analysis of a Fragmenting Sunspot Using Hinode Observations. *ApJ*, *755*, 16. doi:[10.1088/0004-637X/755/1/16](https://doi.org/10.1088/0004-637X/755/1/16). [arXiv:1205.6669](https://arxiv.org/abs/1205.6669).
- Ortiz, A., Bellot Rubio, L. R., & Rouppe van der Voort, L. (2010). Downflows in Sunspot Umbral Dots. *ApJ*, *713*, 1282–1291. doi:[10.1088/0004-637X/713/2/1282](https://doi.org/10.1088/0004-637X/713/2/1282). [arXiv:1003.1897](https://arxiv.org/abs/1003.1897).
- Parker, E. N. (1979). Sunspots and the physics of magnetic flux tubes. IX - Umbral dots and longitudinal overstability. *ApJ*, *234*, 333–347. doi:[10.1086/157501](https://doi.org/10.1086/157501).
- Puschmann, K. G., Denker, C., Kneer, F., Al Erdogan, N., Balthasar, H., Bauer, S. M., Beck, C., Bello González, N., Collados, M., Hahn, T., Hirzberger, J., Hofmann, A., Louis, R. E., Nicklas, H., Okunev, O., Martínez Pillet, V., Popow, E., Seelemann, T., Volkmer, R., Wittmann, A. D., & Woche, M. (2012). The GREGOR Fabry-Pérot Interferometer. *Astronomische Nachrichten*, *333*, 880. doi:[10.1002/asna.201211734](https://doi.org/10.1002/asna.201211734). [arXiv:1210.2921](https://arxiv.org/abs/1210.2921).
- Puschmann, K. G., Ruiz Cobo, B., & Martínez Pillet, V. (2010). A Geometrical Height Scale for Sunspot Penumbrae. *ApJ*, *720*, 1417–1431. doi:[10.1088/0004-637X/720/2/1417](https://doi.org/10.1088/0004-637X/720/2/1417). [arXiv:1007.2779](https://arxiv.org/abs/1007.2779).
- Rimmele, T. (2008). On the Relation between Umbral Dots, Dark-cored Filaments, and Light Bridges. *ApJ*, *672*, 684–695. doi:[10.1086/523702](https://doi.org/10.1086/523702).
- Rimmele, T., & Marino, J. (2006). The Evershed Flow: Flow Geometry and Its Temporal Evolution. *ApJ*, *646*, 593–604. doi:[10.1086/504794](https://doi.org/10.1086/504794).

- Rouppé van der Voort, L., Bellot Rubio, L. R., & Ortiz, A. (2010). Upflows in the Central Dark Lane of Sunspot Light Bridges. *ApJ*, 718, L78–L82. doi:[10.1088/2041-8205/718/2/L78](https://doi.org/10.1088/2041-8205/718/2/L78). [arXiv:1006.4578](https://arxiv.org/abs/1006.4578).
- Ruiz Cobo, B., & Asensio Ramos, A. (2013). Returning magnetic flux in sunspot penumbrae. *A&A*, 549, L4. doi:[10.1051/0004-6361/201220373](https://doi.org/10.1051/0004-6361/201220373). [arXiv:1211.6335](https://arxiv.org/abs/1211.6335).
- Ruiz Cobo, B., & del Toro Iniesta, J. C. (1992). Inversion of Stokes profiles. *ApJ*, 398, 375–385. doi:[10.1086/171862](https://doi.org/10.1086/171862).
- Scharmer, G. B., de la Cruz Rodriguez, J., Sütterlin, P., & Henriques, V. M. J. (2013). Opposite polarity field with convective downflow and its relation to magnetic spines in a sunspot penumbra. *A&A*, 553, A63. doi:[10.1051/0004-6361/201220899](https://doi.org/10.1051/0004-6361/201220899). [arXiv:1211.5776](https://arxiv.org/abs/1211.5776).
- Schleicher, H., Balthasar, H., & Wöhl, H. (2003). Velocity Field of a Complex Sunspot with Light Bridges. *Sol. Phys.*, 215, 261–280. doi:[10.1023/A:1025688927043](https://doi.org/10.1023/A:1025688927043).
- Schüssler, M., & Vögler, A. (2006). Magnetoconvection in a Sunspot Umbra. *ApJ*, 641, L73–L76. doi:[10.1086/503772](https://doi.org/10.1086/503772). [arXiv:astro-ph/0603078](https://arxiv.org/abs/astro-ph/0603078).
- Sobotka, M., & Jurčák, J. (2009). Evolution of Physical Characteristics of Umbral Dots and Penumbra Grains. *ApJ*, 694, 1080–1084. doi:[10.1088/0004-637X/694/2/1080](https://doi.org/10.1088/0004-637X/694/2/1080).
- van Noort, M. (2012). Spatially coupled inversion of spectropolarimetric image data. I. Method and first results. *A&A*, 548, A5. doi:[10.1051/0004-6361/201220220](https://doi.org/10.1051/0004-6361/201220220). [arXiv:1210.4636](https://arxiv.org/abs/1210.4636).
- Westendorp Plaza, C., del Toro Iniesta, J. C., Ruiz Cobo, B., & Martínez Pillet, V. (2001a). Optical Tomography of a Sunspot. III. Velocity Stratification and the Evershed Effect. *ApJ*, 547, 1148–1158. doi:[10.1086/318377](https://doi.org/10.1086/318377).
- Westendorp Plaza, C., del Toro Iniesta, J. C., Ruiz Cobo, B., Martínez Pillet, V., Lites, B. W., & Skumanich, A. (2001b). Optical Tomography of a Sunspot. II. Vector Magnetic Field and Temperature Stratification. *ApJ*, 547, 1130–1147. doi:[10.1086/318376](https://doi.org/10.1086/318376).